

Counterion-Induced Swelling of Ionic Microgels

Alan R. Denton* and Qiyun Tang†

Department of Physics, North Dakota State University, Fargo, ND 58108-6050, USA

Ionic microgel particles, when dispersed in a solvent, swell to equilibrium sizes that are governed by a balance between electrostatic and elastic forces. Tuning of particle size by varying external stimuli, such as pH , salt concentration, and temperature, has relevance for drug delivery, microfluidics, and filtration. To model swelling of ionic microgels, we derive a statistical mechanical theorem, which proves exact within the cell model, for the electrostatic contribution to the osmotic pressure inside a permeable colloidal macroion. Applying the theorem, we demonstrate how the distribution of counterions within an ionic microgel determines the internal osmotic pressure. By combining the electrostatic pressure, which we compute via both Poisson-Boltzmann theory and molecular dynamics simulation, with the elastic pressure, modeled via the Flory-Rehner theory of swollen polymer networks, we show how deswelling of ionic microgels with increasing concentration of particles can result from a redistribution of counterions that reduces electrostatic pressure. A linearized approximation for the electrostatic pressure, which proves remarkably accurate, provides physical insight and greatly eases numerical calculations for practical applications. Comparing with experiments, we explain why soft particles in deionized suspensions deswell upon increasing concentration and why this effect may be suppressed at higher ionic strength. The failure of the uniform ideal-gas approximation to adequately account for counterion-induced deswelling below close packing of microgels is attributed to neglect of spatial variation of the counterion density profile and the electrostatic pressure of incompletely neutralized macroions.

I. INTRODUCTION

Soft colloids, including star polymers, microgels, block-copolymer micelles, dendrimers, and emulsion droplets, have attracted broad attention in recent years for their rich and tunable materials properties [1]. Experimental and modeling studies have explored elastic properties of single particles [2–18] and phase behavior and dynamics of bulk suspensions [19–30]. Particular interest has focused on microgels [31–34] – microscopic gel particles, composed of porous, elastic networks of cross-linked polymers, swollen by a solvent [35–38]. Well-characterized microgels have been synthesized by emulsion polymerization and cross-linking of polyelectrolytes, such as poly(N-isopropylacrylamide) (PNIPAM) [39–41] and poly-vinylpyridine [6, 7].

When dispersed in water, microgels can acquire charge by releasing counterions into solution. Permeability to solvent molecules and small ions drives competition between elastic and electrostatic forces. Swelling and equilibrium particle size can be controlled by adjusting temperature, pH , and ionic strength, leading to tunable properties and making ionic microgels appealing for chemical sensing and drug delivery [42–46]. Recent reviews describe applications in the chemical, biomedical, food, consumer care, pharmaceutical, and petroleum industries [31, 32].

Physical properties of microgel suspensions have been measured by light and small-angle neutron scattering, confocal microscopy, and osmometry, probing connec-

tions between particle elasticity, osmotic pressure, structure, and thermodynamic phase behavior [47–55]. Efforts to model ionic microgels have focused on microion distributions, effective electrostatic interactions between macroions, and associated thermodynamic phase behavior [26–28, 56–60]. Computer simulations of the primitive model of polyelectrolyte solutions and of coarse-grained bead-spring models of polyelectrolyte networks [61–65] have been essential in guiding theoretical developments. Despite recent progress in linking single-particle properties with bulk behavior of ionic microgel suspensions, important challenges remain. In particular, the influence of counterions on the osmotic pressure inside of permeable, compressible macroions and on equilibrium particle size is not fully understood.

While numerous experimental studies have explored the effect of salt concentration on swelling of ionic microgels [66–71], relatively few have examined the influence of particle concentration [4, 5, 7–10]. Borrega *et al.* [4] and Tan *et al.* [9] deduced particle sizes from viscosity measurements and demonstrated that free counterions in solution can induce osmotic deswelling of microgels in dense suspensions. Cloitre *et al.* [5] used dynamic light scattering (DLS) to quantify variations in hydrodynamic radius with cross-linker density and degree of ionization of polyelectrolyte microgels, synthesized from ethyl acrylate and methacrylic acid monomers, and proposed that free counterions may induce deswelling at microgel concentrations approaching close packing. Pelaez-Fernandez *et al.* [7] measured the osmotic pressure of suspensions of cross-linked poly-vinylpyridine microgels via osmometry and dialysis. Over a range of concentrations, from dilute to near hard-sphere freezing, they obtained pressures in excess of what could be reasonably attributed to the microgel particles alone. They explained their results

* alan.denton@ndsu.edu

† Current address: Institut für Theoretische Physik, Georg-August Universität, 37077 Göttingen, Germany

by hypothesizing a dominant influence of free counterions in solution. Like Cloitre *et al.*, they observed significant deswelling only at concentrations near close packing. Romeo *et al.* [8], using DLS to measure the hydrodynamic radius of relatively stiff PNIPAM particles over a range of concentrations, concluded that any counterion-induced shrinkage is negligible. In contrast, Holmqvist *et al.* [10] observed much stronger deswelling of loosely cross-linked PNIPAM-co-PAA particles in deionized suspensions.

Measurements of ionic microgel particle sizes are commonly interpreted in the dilute regime via scaling theories, originally developed for macroscopic gels [72–78], which assume strict electroneutrality and total confinement of counterions to the gel, or via phenomenological models [2–8], which allow local deviations from electroneutrality and partial release of counterions. Both approaches, by approximating the counterions as a uniformly distributed ideal gas, neglect continuous variation in the counterion density, which can be important for accurately modeling swelling of microscopically sized gel particles. To our knowledge, no previous studies have realistically modeled the direct relationship between the counterion density profile, osmotic pressure, and swelling of ionic microgels.

In this paper, we present a rigorous analysis of the dependence of ionic microgel size on counterion distribution and on the bulk concentration of particles. By coupling elasticity theory of cross-linked gel networks with a new statistical mechanical theorem for the electrostatic contribution to the internal osmotic pressure, we demonstrate how the counterion distribution determines the equilibrium size of ionic microgels. Through a combination of theory and simulation, we explain experimentally observed density-dependent deswelling and identify system parameters for which such effects can be enhanced. Thus, we predict that sufficiently soft and ionized microgels can penetrate apertures considerably narrower than their dilute size at concentrations below close-packing, with potentially important implications for drug delivery [79], microfluidics [17, 34, 80], and filtration [81, 82].

II. MODELS

A. Microgel Suspension

We consider a suspension of soft, charged colloidal particles (macroions), permeable to water and microions. Common examples are polyelectrolyte microgels and capsules dispersed in an aqueous electrolyte. Within the primitive model of polyelectrolytes, the solvent is reduced to a dielectric continuum of dielectric constant ϵ . For simplicity, we assume ϵ to be the same inside and outside of the macroion. This assumption can be easily relaxed to allow for nonuniform dielectric constant. We further assume spherical macroions, of dry (collapsed) radius a_0 , swollen radius a , and charge number (valence) Z associ-

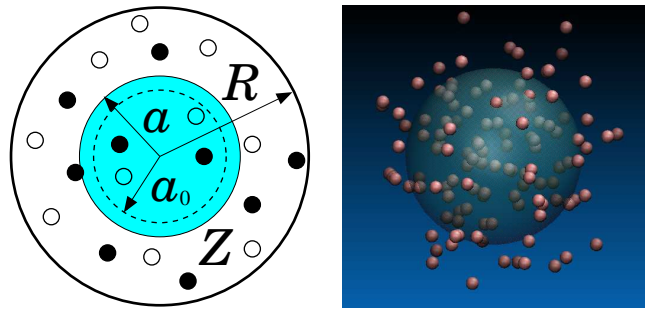


FIG. 1. Left: Cell model with ionic microgel of swollen radius a (dry radius a_0) and valence Z centered in a spherical cell of radius R along with microions. Right: Snapshot from MD simulation of an ionic microgel and counterions.

ated with a fixed charge distribution, $n_f(r)$, which varies only with radial distance r from the center. The fixed charge comes from dissociation of Z counterions, which can contribute to the osmotic pressure by virtue of their freedom to move throughout the system. Any counterions that may be immobilized by condensation onto polyelectrolyte chains [83] are excluded from this count. It is important to note that this bare charge number can be substantially higher than the effective charge number associated with interparticle pair interactions, as is deduced from light scattering experiments [10]. The counterions and salt ions (microions) are modeled as point charges, of valence $\pm z$, that can freely penetrate the macroions. In equilibrium, the microions distribute themselves so as to equalize the chemical potential throughout the system.

In Donnan equilibrium, microions can exchange with a salt reservoir, of bulk microion pair concentration n_0 , through an immovable, semipermeable membrane, which is impermeable to macroions, but permeable to both microions and solvent. Equality of chemical potentials entails a nonuniform distribution of ions between the suspension and reservoir and a corresponding osmotic pressure, i.e., a difference in bulk pressure between the suspension and the reservoir, which is sustained by a counteracting force exerted by the externally fixed membrane.

Within the suspension, microions can also exchange between the interior and exterior macroion regions. The periphery of a macroion thus acts analogously to a semipermeable membrane, allowing microions to penetrate, but holding the fixed charge within the macroion. In this internal Donnan equilibrium, the fixed charge on the polyelectrolyte chains creates a nonuniform distribution of microions that equalizes the chemical potential. The interior microion gas and the self-repulsion of the fixed charge within the macroion combine to generate an outward electrostatic pressure that swells the macroion. Swelling is limited by the inward elastic restoring forces exerted by the cross-linked gel. In equilibrium, a balance between these opposing pressures determines the average macroion size. As will become apparent below, the electrostatic contributions to the pressure inside and outside a microgel differ.

B. Cell Model

The cell model [84] centers a single macroion in a spherical cell along with N mobile microions (see Fig. 1). The Hamiltonian of the system, $H = H_e + H_g$, decouples naturally into an electrostatic component H_e , which incorporates all Coulomb interactions in the cell, and a gel component H_g , which describes the elastic and mixing degrees of freedom of a polymer network. The electrostatic component can be further decomposed as follows:

$$H_e = U_m(a) + U_{m\mu}(\{\mathbf{r}\}; a) + U_{\mu\mu}(\{\mathbf{r}\}) , \quad (1)$$

where $U_m(a)$ is the macroion self-energy and $U_{m\mu}(\{\mathbf{r}\}; a)$ and $U_{\mu\mu}(\{\mathbf{r}\})$ are the macroion-microion and microion-microion interaction energies, respectively, which depend on the ion coordinates, $\{\mathbf{r}_1, \dots, \mathbf{r}_N\} \equiv \{\mathbf{r}\}$. Note that only the first two terms in Eq. (1) depend on the macroion radius. The macroion-microion interaction may be expressed as

$$U_{m\mu}(\{\mathbf{r}\}; a) = \sum_{i=1}^N v_{m\mu}(\mathbf{r}_i; a) , \quad (2)$$

where $v_{m\mu}(\mathbf{r}; a)$ is the macroion-microion pair potential. Although the cell model completely neglects macroion-macroion correlations, the relative contribution of such interparticle correlations to osmotic pressure is known to be weakest in the low-salt limit [85, 86], thus resulting in quite an accurate representation of deionized microgel suspensions [60–62]. Furthermore, independent simulations of many microgel particles, interacting via a repulsive Hertz pair potential and fluctuating in size, reveal that for the same elastic parameters as considered here, macroion-macroion correlations and steric interactions begin to significantly affect swelling only at average volume fractions approaching close packing [87].

III. THEORY

A suspension that is free to exchange microions with a salt reservoir through a semipermeable membrane is best represented in the semi-grand canonical ensemble. Decoupling of the electrostatic and gel components of the Hamiltonian implies a factorization of the semi-grand canonical partition function, $\Xi = \Xi_e \mathcal{Z}_g$, into an electrostatic grand canonical partition function Ξ_e and a gel canonical partition function \mathcal{Z}_g . Correspondingly, the semi-grand potential, $\Omega = -k_B T \ln \Xi = \Omega_e + F_g$, separates conveniently into an electrostatic grand potential, $\Omega_e = -k_B T \ln \Xi_e$, and a gel Helmholtz free energy, $F_g = -k_B T \ln \mathcal{Z}_g$. We focus first on the electrostatic grand canonical partition function, in a spherical cell of fixed radius R , which can be expressed as

$$\Xi_e(\mu_0, a, R, T) \propto \sum_{N=0}^{\infty} \frac{e^{\beta \mu_0 N}}{N!} \prod_{i=1}^N \int_0^R dr_i r_i^2 e^{-\beta H_e} , \quad (3)$$

with $\beta \equiv 1/(k_B T)$ at temperature T and $\mu_0 = k_B T \ln n_0$ the microion chemical potential in the reservoir.

The bulk osmotic pressure – the pressure in the suspension relative to the pressure in the reservoir – is defined via the derivative of the grand potential with respect to the system volume, $V = 4\pi R^3/3$:

$$\pi_b = - \left(\frac{\partial \Omega}{\partial V} \right)_{\mu_0, a, T} = \frac{k_B T}{4\pi R^2} \frac{\partial}{\partial R} \ln \Xi_e(\mu_0, a, R, T) , \quad (4)$$

where on the right side we have used the fact that \mathcal{Z}_g is independent of R in the cell model. Substituting for $\Xi_e(\mu_0, a, R, T)$ from Eqs. (1)–(3) yields

$$\beta \pi_b = \langle n_+(R) \rangle + \langle n_-(R) \rangle , \quad (5)$$

where $n_{\pm}(R)$ are the microion densities at the cell boundary and $\langle \rangle$ denotes an ensemble average over microion coordinates. This classic theorem for the bulk osmotic pressure was first derived within PB theory [84], but proves exact within the cell model [88].

Similarly, the internal osmotic pressure – the pressure inside the macroions relative to the bulk osmotic pressure – can be defined via a derivative of Ω with respect to the single-macroion volume, $v = 4\pi a^3/3$:

$$\pi_{in} = - \left(\frac{\partial \Omega}{\partial v} \right)_{\mu_0, R, T} = \frac{k_B T}{4\pi a^2} \frac{\partial}{\partial a} \ln \Xi(\mu_0, a, R, T) . \quad (6)$$

More explicitly, π_{in} is the excess of the osmotic pressure inside a macroion over the osmotic pressure π_b outside, within the suspension. In equilibrium, the electrostatic pressure is balanced by the elastic pressure of the polymer gel, resulting in $\pi_{in} = 0$. Upon substituting $\Omega = \Omega_e + F_g$ into Eq. (6), the internal osmotic pressure separates into electrostatic and gel contributions: $\pi_{in} = \pi_e + \pi_g$. From Eqs. (1)–(3), the electrostatic contribution to the internal osmotic pressure may be expressed as

$$\pi_e = - \frac{1}{4\pi a^2} \left(\frac{\partial}{\partial a} U_m(a) + \left\langle \frac{\partial}{\partial a} U_{m\mu}(a) \right\rangle \right) . \quad (7)$$

For the gel contribution, we invoke the Flory-Rehner theory of gel elasticity [18, 72], which combines mixing entropy, polymer-solvent interactions, and elastic network energy to predict a gel free energy

$$\beta F_g = N_m [(\alpha^3 - 1) \ln(1 - \alpha^{-3}) + \chi(1 - \alpha^{-3})] + \frac{3}{2} N_{ch} (\alpha^2 - \ln \alpha - 1) , \quad (8)$$

where $\alpha \equiv a/a_0$ is the particle swelling ratio, N_m and N_{ch} are the numbers of monomers and chains per microgel, and χ is the Flory solvency parameter. The corresponding gel pressure is given by

$$\beta \pi_g v = - N_m [\alpha^3 \ln(1 - \alpha^{-3}) + \chi \alpha^{-3} + 1] - N_{ch} (\alpha^2 - 1/2) . \quad (9)$$

At equilibrium swelling, the semi-grand potential is a minimum with respect to variation of α , which is equivalent to vanishing of the total internal osmotic pressure: $\pi_{\text{in}}(\alpha) = \pi_e(\alpha) + \pi_g(\alpha) = 0$. From this stability criterion, we explore equilibrium swelling as a function of particle concentration in Sec. V.

Our theorem for the electrostatic pressure difference across the surface of a permeable macroion [Eq. (7)] is exact within the cell model. Practical implementation now requires a model for the fixed charge distribution within a macroion. To illustrate, we proceed with the simplest model of a uniformly charged microgel of fixed charge number density $n_f(r) = Z/v$ ($r \leq a$). In this case, the energy of interaction between a macroion and a microion of valence z is given by

$$\beta v_{m\mu}(r) = -\frac{Zz\lambda_B}{2a} (3 - r^2/a^2), \quad r \leq a, \quad (10)$$

and the macroion self-energy is

$$\beta U_m = \frac{3}{5} Z^2 \frac{\lambda_B}{a}, \quad (11)$$

where $\lambda_B \equiv e^2/(\epsilon k_B T)$ is the Bjerrum length. From Eq. (10), it follows that

$$\beta \left\langle \frac{\partial}{\partial a} U_{m\mu}(a) \right\rangle = -\frac{Z\lambda_B}{2} \left\langle \frac{\partial}{\partial a} \sum_{i=1}^N z_i \left(\frac{3}{a} - \frac{r_i^2}{a^3} \right) \right\rangle, \quad (12)$$

with $z_i = \pm z$ denoting the valence of microion i . Now substituting Eq. (12) into Eq. (7) yields

$$\beta \pi_e v = \frac{Z\lambda_B}{2a} \left(\frac{2}{5} Z - \langle N_+ \rangle + \langle N_- \rangle + \frac{\langle r^2 \rangle_+ - \langle r^2 \rangle_-}{a^2} \right). \quad (13)$$

where, for given radial number density profiles $n_{\pm}(r)$,

$$\langle N_{\pm} \rangle = 4\pi \int_0^a dr r^2 n_{\pm}(r) \quad (14)$$

are the mean numbers of interior counterions/coions and

$$\langle r^2 \rangle_{\pm} = 4\pi \int_0^a dr r^4 n_{\pm}(r) \quad (15)$$

are second moments of the interior microion density profiles. Equation (13) provides an explicit formula – exact within the spherical cell model – for the electrostatic contribution to the internal osmotic pressure of an ionic microgel modeled as a uniformly charged sphere. This result may be easily generalized to other macroion architectures, such as core-shell microgels and polyelectrolyte capsules. Implementing Eq. (13) requires the microion density profiles inside of the macroion, which may be obtained from either theory or simulation. In the next section, we discuss computational methods for computing microion densities and osmotic pressure.

IV. COMPUTATIONAL METHODS

A. Nonlinear Poisson-Boltzmann Theory

To explicitly compute the electrostatic contribution to the osmotic pressure internal to ionic microgel particles, we implemented Poisson-Boltzmann (PB) theory within the spherical cell model [84, 88, 89]. The Poisson equation for the electrostatic potential $\psi(r)$ (in $k_B T/e$ units),

$$\nabla^2 \psi(r) = -4\pi \lambda_B [n_+(r) - n_-(r) - n_f(r)], \quad (16)$$

combined with the mean-field Boltzmann approximation for the equilibrium microion densities,

$$n_{\pm}(r) = n_0 \exp[\mp \psi(r)], \quad (17)$$

yields the nonlinear PB equation,

$$\psi''(r) + \frac{2}{r} \psi'(r) = \begin{cases} \kappa_0^2 \sinh \psi(r) + \frac{3Z\lambda_B}{a^3}, & 0 < r \leq a \\ \kappa_0^2 \sinh \psi(r), & a < r \leq R, \end{cases} \quad (18)$$

where $\kappa_0 = \sqrt{8\pi \lambda_B n_0}$ is the Debye screening constant in the electrolyte reservoir. Solving Eq. (18), with boundary conditions $\psi'(0) = \psi'(R) = 0$, yields $\psi(r)$ and thus $n_{\pm}(r)$ [60], from which we compute the electrostatic pressure via Eqs. (13)-(15). The electrostatic pressure may also be computed from the electrostatic grand potential,

$$\beta \Omega_e = 4\pi \int_0^R dr r^2 \sum_{i=\pm} n_i(r) \left[\ln \left(\frac{n_i(r)}{n_0} \right) - 1 \right] + \frac{1}{2\lambda_B} \int_0^R dr r^2 |\psi'(r)|^2, \quad (19)$$

by taking a derivative with respect to a :

$$\pi_e = -\frac{1}{4\pi a^2} \left(\frac{\partial}{\partial a} \Omega_e(\mu_0, a, R, T) \right)_{\mu_0, R, T}. \quad (20)$$

B. Linearized Approximation

For comparison with the nonlinear PB theory, we also consider a linearized approximation that provides convenient analytical expressions. For a suspension of spherical, uniformly charged microgels with average microion densities n_{\pm} , linear response theory [56, 60] predicts microion density profiles (to within a constant)

$$n_{\pm}(r) = \pm \frac{Z}{v} \frac{n_{\pm}}{n_{\mu}} \begin{cases} 1 - \frac{1 \pm x}{x} e^{-x} \frac{a}{r} \sinh \left(\frac{xr}{a} \right), & r \leq a \\ \left(\cosh x - \frac{\sinh x}{x} \right) \frac{a}{r} e^{-xr/a}, & r > a, \end{cases} \quad (21)$$

where $n_{\mu} = n_+ + n_-$ is the total average microion density, $x = \kappa a$, and $\kappa = \sqrt{4\pi \lambda_B n_{\mu}}$ is the screening constant in the suspension (*cf.* κ_0 in the reservoir). For a suspension

of average microgel and salt densities n_m and n_s , respectively, electroneutrality dictates $n_\mu = Zn_m + 2n_s$. Substituting Eq. (21) into Eqs. (14) and (15) yields (to within a constant) the mean numbers of interior microions,

$$\langle N_\pm \rangle = \pm Z \frac{n_\pm}{n_\mu} \left[1 - 3 \frac{1+x}{x^3} e^{-x} (x \cosh x - \sinh x) \right], \quad (22)$$

and second moments of interior microion density profiles,

$$\langle r^2 \rangle_\pm = \pm \frac{3}{5} Z a^2 \frac{n_\pm}{n_\mu} \left\{ 1 - 5 \frac{1+x}{x^5} e^{-x} \times [x(x^2 + 6) \cosh x - 3(x^2 + 2) \sinh x] \right\}. \quad (23)$$

Finally, combining Eqs. (22), (23), and (13) yields

$$\beta \pi_e v = 3Z^2 \frac{\lambda_B}{a} \frac{1+x}{x^4} e^{-x} \left(\frac{1+x^2}{x} \sinh x - 3 \cosh x \right). \quad (24)$$

This analytical approximation, which proves to be quite accurate, greatly eases calculations and facilitates comparisons with experiments (see Sec. V).

C. Molecular Dynamics Simulations

In addition to applying PB theory, we also performed molecular dynamics (MD) simulations within the spherical cell model. Using the LAMMPS molecular simulator [90, 91], we confined a fixed number of monovalent point counterions – interacting via Coulomb pair potentials – to a spherical cell of fixed radius by a repulsive Lennard-Jones wall force. We modeled the influence of the macroion on the counterions by imposing an “external” electric field equal to the negative gradient of Eq. (10) and maintained a constant average temperature via a Nosé-Hoover thermostat. The canonical (constant- NVT) ensemble proves more practical here than the grand canonical ensemble and yields the same microion distributions for the same system salt concentration [61, 62, 88]. Following equilibration for 10^6 steps, we computed thermodynamic quantities by averaging over particle trajectories for 10^7 time steps. From the resulting histogram of the counterion density, we computed $\langle N_+ \rangle$ and $\langle r^2 \rangle_+$, and then π_e from Eq. (13).

V. RESULTS AND DISCUSSION

A. Illustrative Example

As noted above, the interior pressure theorem [Eq. (7)] can be applied to predict the electrostatic contribution to the osmotic pressure within macroions of any architecture, including those with nonuniform cross-linker density, such as core-shell [3, 8, 10, 18, 51, 92] or hollow [93] microgels. To illustrate the implementation of

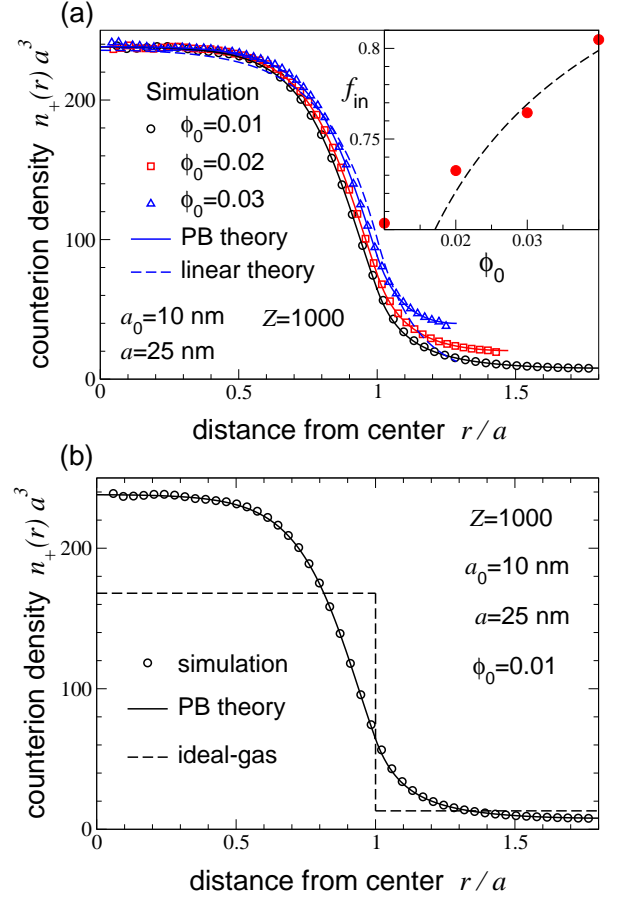


FIG. 2. (a) Counterion number density profiles near an ionic microgel of dry radius $a_0 = 10$ nm, swollen radius $a = 25$ nm, and valence $Z = 1000$ in a salt-free aqueous solution from MD simulations (symbols) and PB theory (solid curves) in the cell model at dry particle volume fractions $\phi_0 = 0.01, 0.02, 0.03$. Also shown is the prediction of linear response theory [56] (dashed curve) for $\phi_0 = 0.03$. Inset: Average fraction of counterions inside a macroion, f_{in} vs. ϕ_0 , from simulations (symbols) and linear response theory (curve). (b) Counterion density profile predicted by PB theory (solid curve) compared with uniform ideal-gas approximation (dashed curve).

the theorem, we present numerical results, in the spherical cell model, for a uniformly charged microgel of dry radius $a_0 = 10$ nm, swollen radius $a = 25$ nm, and valence $Z = 1000$ in a salt-free aqueous solution at $T = 293$ K ($\lambda_B = 0.714$ nm). Figure 2(a) shows radial profiles of monovalent counterion density for dry particle volume fractions $\phi_0 \equiv (a_0/R)^3 = 0.01, 0.02, 0.03$, corresponding to swollen particle volume fractions $\phi \equiv (a/R)^3 = \alpha^3 \phi_0 = 0.156, 0.313, 0.469$. The counterion density profiles are relatively flat near the microgel center, where the electric field is weak, and fall off toward the periphery over a distance comparable to the screening length, κ^{-1} in the salt-free limit [see Eq. (21)]. Close agreement between simulation and theory validates the PB approximation. Also shown in Fig. 2(a) is the linearized approximation for $\phi_0 = 0.03$, which proves quite

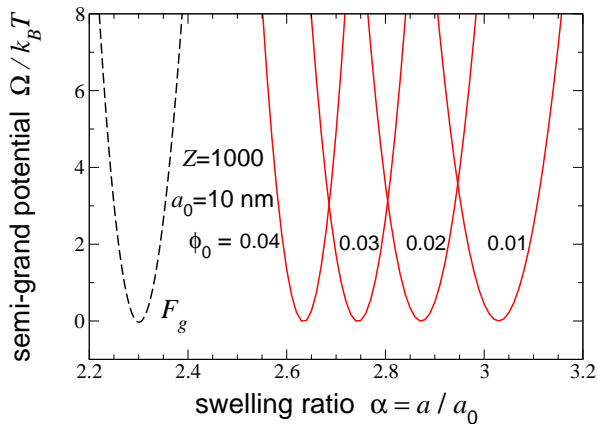


FIG. 3. Semi-grand potential Ω vs. particle swelling ratio α of ionic microgels with valence $Z = 1000$, dry particle radius $a_0 = 10$ nm, $N_m = 2 \times 10^5$ monomers, $N_{ch} = 100$ chains, and $\chi = 0.5$ in deionized solutions of dry particle volume fractions $\phi_0 = 0.01 - 0.04$ (right to left). To ease comparison, the minima are shifted to zero. For reference, the free energy F_g of a nonionic microgel [Eq. (8)] is also shown (dashed curve).

accurate, aside from slight deviations near the particle periphery. For comparison, Fig. 2(b) shows the counterion density profile assumed by the uniform ideal-gas approximation (see Sec. V).

From the simulations, we also extracted the average fraction of interior mobile counterions, $f_{in} = \langle N_+ \rangle / Z$. Integrating the PB counterion density profile over the microgel volume gave nearly identical results. The inset of Fig. 2 shows that 20-30% of the counterions reside outside of the macroion, confirming that bulk theories of polyelectrolyte gels, which assume total counterion confinement, are not applicable here. Over this range of volume fractions ($\phi_0 = 0.01-0.04$, $\phi = 0.156-0.625$), the average fraction of interior counterions is seen to increase monotonically and roughly linearly. A similar trend results from the linearized approximation [Eq. (22)], which proves to be accurate for $\phi_0 > 0.02$ ($\phi > 0.3$). Deviations at lower volume fractions stem from nonlinear screening and differences in boundary conditions between the two theories (free vs. cell boundary conditions) [56, 60].

Proceeding to the osmotic pressure, we computed π_e by solving the nonlinear PB equation [Eq. (18)] for $n_{\pm}(r)$ and substituting $\langle N_{\pm} \rangle$ and $\langle r^2 \rangle_{\pm}$ into Eq. (13). As a consistency check, we also computed π_e numerically from Eq. (20), using the PB solution for the counterion density profile, and obtained results identical to those from Eq. (13). We emphasize, however, that Eq. (20), because it relies on knowledge of the grand potential, is in practice limited to PB theory [27]. In contrast, our internal pressure theorem [Eqs. (7) and (13)] can be used to extract the osmotic pressure also from simulations, which naturally include correlations between microions.

To explore the equilibrium particle size, we combined the electrostatic contribution to the grand potential and internal osmotic pressure, which promotes mi-

crogel swelling, with the elastic gel contribution, which limits swelling. For illustration, we present results of our calculations for particles characterized by $a_0 = 10$ nm, $Z = 1000$, $N_m = 2 \times 10^5$, $N_{ch} = 100$, and $\chi = 0.5$, representing moderately charged, loosely cross-linked gels comprising monomers of diameter 3 Å. Note that the ratio $Z/N_m = 0.005$ is well below the threshold for counterion condensation onto polyelectrolyte chains [83]. Such relatively small microgels contain still a sufficiently high number of monomers to be reasonably modeled by a continuous charge distribution, especially considering that thermal motions of the chains tend to wash out charge discreteness. Nevertheless, direct comparison of our predictions with data from simulations of microscopic models with discrete charges would help to clarify any limitations of the continuum model. Furthermore, our purpose here is merely to test the accuracy of the theory against MD simulations for the same model. After validating the theory, we compare predictions with experimental data for much larger microgels carrying much higher charge numbers (see Sec. VB).

Variation of the Flory-Rehner free energy [Eq. (8)] with swelling ratio implies thermally excited fluctuations in particle size, i.e., dynamical polydispersity. An isolated nonionic microgel has an equilibrium size that fluctuates according to a probability distribution,

$$P(\alpha) \propto \exp[-\beta F_g(\alpha)], \quad (25)$$

the most probable size then corresponding to the minimum of $F_g(\alpha)$. In the case of ionic microgels, mobile counterions generate an internal electrostatic pressure that modifies this size distribution and enhances swelling.

Results for the semi-grand potential [from Eqs. (8) and (19)] are shown in Fig. 3 over a range of dry particle volume fractions. To facilitate comparison, the minimum values of Ω are shifted to zero. For these system parameters, the electrostatic pressure evidently produces significant swelling, while at the same time broadening the particle size distribution by shifting the minimum of $\Omega(\alpha)$ out to a range of α with weaker curvature. With increasing particle concentration, however, swelling is reduced and the size polydispersity narrows. As the dry particle volume fraction increases from 0.01 to 0.04, the swollen particle volume fraction increases as well, despite deswelling, although more gradually, from 0.28 to 0.73. Nevertheless, it is essential to realize that the particle deswelling and narrowing polydispersity predicted here are driven only by a redistribution of counterions, not by correlations between microgels, which are neglected in the cell model. At sufficiently high concentrations of microgels, electrostatic and steric interactions between particles will eventually affect the size distribution.

In Fig. 4(a), we plot the electrostatic contribution to the internal osmotic pressure (relative to the suspension) vs. swelling ratio, as calculated from both theory and simulation. For comparison, the osmotic pressure in the suspension (relative to the reservoir) is also plotted. These results were computed via Eqs. (5) and (13), using coun-

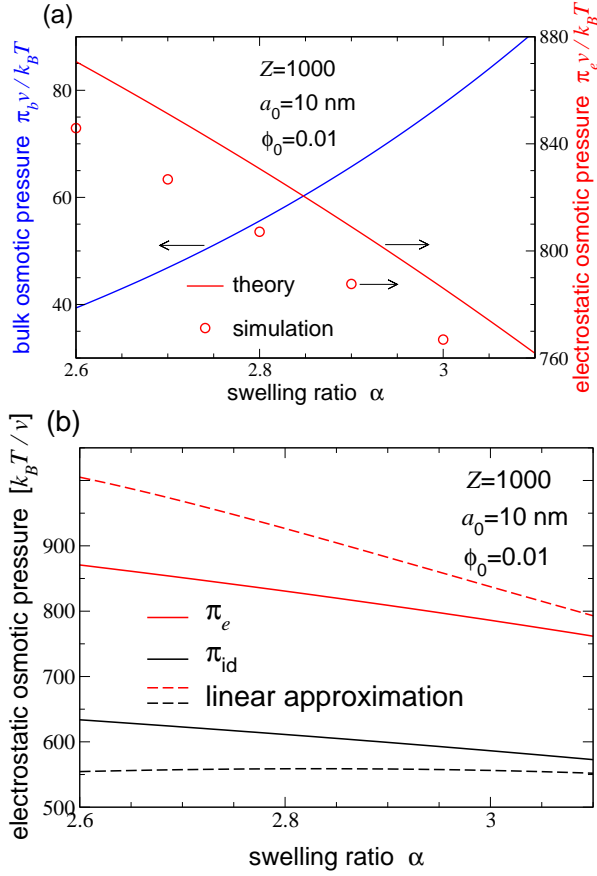


FIG. 4. (a) Osmotic pressure in bulk suspension π_b relative to reservoir (left) [Eq. (5)] and electrostatic contribution to internal osmotic pressure π_e relative to suspension (right) [Eq. (13)] vs. particle swelling ratio α for valence $Z = 1000$, dry particle radius $a_0 = 10$ nm, and dry particle volume fraction $\phi_0 = 0.01$. Curves are from PB theory and symbols from MD simulations in the cell model. (b) Electrostatic contribution to internal osmotic pressure π_e (red curves), uniform ideal-gas approximation π_{id} [Eq. (26)] (black curves), and linear response approximations [Eqs. (22) and (24)] (dashed).

terion density profiles calculated from PB theory and extracted as histograms from the simulations. For the internal electrostatic pressure, PB theory and MD simulation agree to within 3%, providing a consistency check and validating the mean-field Boltzmann approximation. With increasing swelling ratio, π_b increases monotonically with swelling ratio, as the counterion density outside the microgels grows with increasing volume fraction (see Fig. 2). At the same time, π_e decreases monotonically with increasing α , due to a declining charge density with increasing particle volume.

In Fig. 4(b), we plot the total electrostatic contribution to the internal osmotic pressure vs. swelling ratio together with the linear response approximation, which proves reasonable and increasingly accurate with increasing α (and ϕ). Also shown in Fig. 4(b) is the uniform

ideal-gas approximation,

$$\beta \pi_{id} v = Z \left(f_{in} - (1 - f_{in}) \frac{\phi}{1 - \phi} \right), \quad (26)$$

which is commonly used as an estimate of π_e when interpreting experimental data [2–10]. For these parameters, this approximation is seen to significantly underestimate the magnitude of the electrostatic contribution to the internal osmotic pressure. This disparity is perhaps not surprising, given that such a relatively small microgel is far from electroneutral. In qualitative terms, a physical explanation for the differing predictions of the two approaches is that the uniform ideal-gas approximation neglects, not only the spatial variation of the counterion density profile, as illustrated in Fig. 2(b), but also the outward electrostatic pressure of the incompletely neutralized macroion.

The electrostatic and elastic contributions to the internal osmotic pressure are juxtaposed in Fig. 5(a) over a range of dry volume fractions. We computed the elastic contribution from Eq. (9) and the electrostatic contribution from Eq. (13), using the counterion distributions determined from both PB theory [Eq. (18)] and MD simulation. Close agreement between theory and simulation again provides a consistency check on our calculations. With increasing dry volume fraction, the electrostatic pressure monotonically decreases, consistent with the shift in the semi-grand potential minimum. This decrease in outward pressure, again arising from a redistribution of counterions, drives a corresponding reduction in equilibrium particle size. Figure 5(b) shows the equilibrium swelling ratio α , computed as the root of the equation, $\pi_e(\alpha) + \pi_g(\alpha) = 0$, where $\pi_e(\alpha)$ and $\pi_g(\alpha)$ are obtained from Eqs. (13)–(17) and Eq. (9). For these parameters, the equilibrium swelling ratio drops by more than 10% from dilute to concentrated suspensions.

As a test, we also applied the linearized approximation, computing π_e from Eq. (24). As seen in Fig. 5(b), this approximation proves remarkably accurate. It is important to note that, despite the excellent agreement between PB theory and simulation in the present case of monovalent counterions, deviations can be expected for more strongly correlated multivalent counterions. In such cases, where PB theory fails, the new internal osmotic pressure theorem may prove especially valuable. Our predictions are consistent with experimental observations of weak concentration dependence of deswelling of relatively rigid particles [8], but a stronger effect for softer particles [10]. Next, we compare more directly with experiments.

B. Comparisons with Experiments

To illustrate the practical utility of our approach to modeling internal osmotic pressure, we first compare our predictions of deswelling with experimental data of Holmqvist *et al.* [10], who combined static and dynamic

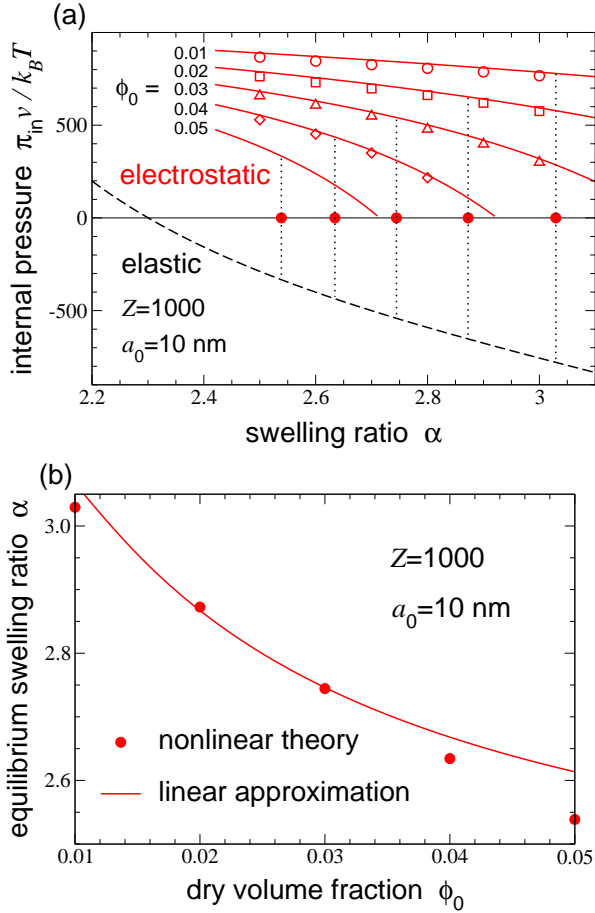


FIG. 5. (a) Contributions to pressure inside ionic microgel vs. particle swelling ratio for the same system parameters as in Fig. 3 and dry particle volume fractions $\phi_0 = 0.01 - 0.05$ (top to bottom). Electrostatic pressure π_e [Eq. (13)] from PB theory (solid curves) and from simulations (open symbols), both in the cell model. Elastic gel pressure π_g (dashed curve) from Flory-Rehner theory [Eq. (9)]. At equilibrium swelling, the total internal osmotic pressure vanishes: $\pi_e(\alpha) + \pi_g(\alpha) = 0$ (filled symbols). (b) Equilibrium swelling ratio vs. ϕ_0 . Symbols: nonlinear PB theory. Curve: linear approximation.

light scattering with integral-equation theory and an effective pair potential model to determine the size and effective charge of PNIPAM-co-PAA core-shell particles as a function of concentration in deionized, pH-neutral solutions. We choose system parameters for maximum consistency with experiments and use corrected microgel concentrations [10] (Erratum). Following the prescribed limit on the number of dissociable groups [10, 47], we take $Z = 3.5 \times 10^4$. In a deionized solution, we set the salt concentration to zero ($n_s = 0$). For the collapsed radius, we use the measured value of $a_0 = 50$ nm. Consistent with particles of this size, comprised of close-packed monomers of radius 0.3 nm, we choose the number of monomers as $N_m = 3 \times 10^6$. Again, $Z/N_m \ll 1$ precludes counterion condensation. To best fit the shape of the distribution, we set the Flory solvency parameter at $\chi = 0.53$, consistent with swollen polymers in water at $T = 20$ °C, and

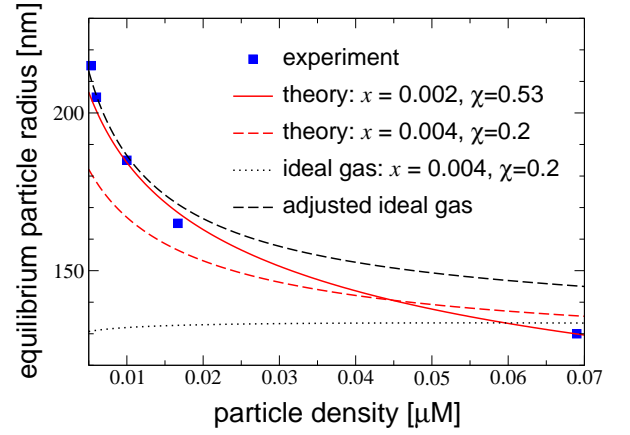


FIG. 6. Equilibrium particle radius vs. number density for PNIPAM-co-PAA microgels of valence $Z = 3.5 \times 10^4$, collapsed radius $a_0 = 50$ nm, and monomer number $N_m = 3 \times 10^6$ in deionized aqueous solution at $T = 20$ °C. Theoretical predictions [Eqs. (9) and (24)] are compared with experiment [10] (symbols) for chain fraction $x = N_{ch}/N_m = 0.002$ and solvency parameter $\chi = 0.53$ (solid red curve) and for $x = 0.004$ and $\chi = 0.2$ (dashed red). Also shown, for comparison, are the ideal-gas approximation [Eqs. (22) and (26)] (dotted black) and a simple adjustment [Eq. (27)] (dashed black) both for $x = 0.004$ and $\chi = 0.2$. From 0.005 to 0.07 μM , the volume fraction varies from $\phi \simeq 0.13$ to 0.39.

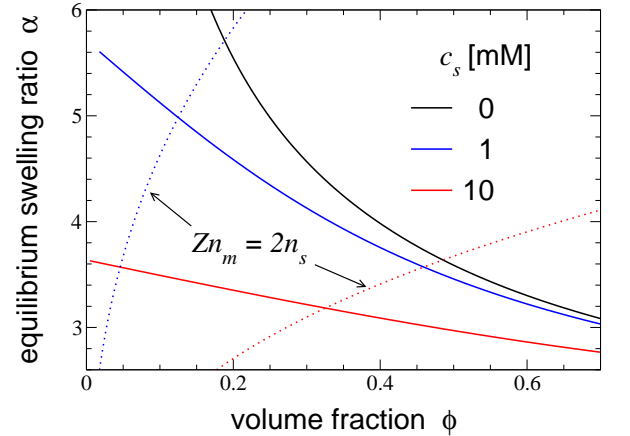


FIG. 7. Equilibrium swelling ratio vs. particle volume fraction for uniform-sphere model of poly-vinylpyridine microgels [6, 7]

of valence $Z = 5 \times 10^6$, collapsed radius $a_0 = 100$ nm, monomer number $N_m = 2 \times 10^8$, chain number $N_{ch} = 4 \times 10^5$, and $\chi = 0.5$ in aqueous solutions at $T = 20$ °C with system salt concentrations $c_s = 0$ (black curve), 1 mM (blue), and 10 mM (red). Along dotted curves, counterion and salt ion densities are equal for $c_s = 1$ mM (blue), $c_s = 10$ mM (red).

neglect any slight concentration dependence [3]. Lacking direct knowledge of the cross-linker density in the shell region, we treat N_{ch} as a fitting parameter.

For particles of this size and charge, the nonlinear PB equation becomes so numerically stiff that our computational method fails to converge to a solution. More

sophisticated iterative methods are then effective [27]. However, in this parameter regime, in which most of the counterions are confined to the nearly electroneutral interior of the macroion, the linear response theory should be reasonably accurate. Thus, we apply the linearized approximation to model the electrostatic contribution to the internal osmotic pressure. As seen in Fig. 6, we obtain a close fit to the experimental data, over a wide range of particle densities, with chain fraction $x \equiv N_{\text{ch}}/N_m = 0.002$, which is consistent with the loosely cross-linked microgel particles in the experiments. To illustrate sensitivity to variation of parameters, we also show the prediction for $x = 0.004$ and $\chi = 0.2$. In general, the equilibrium swelling ratio decreases as x and χ increase, i.e., as the particles become stiffer and the solvent poorer.

For comparison, Fig. 6 also shows the prediction of the uniform ideal-gas approximation, computed as the root of $\pi_{\text{id}} + \pi_g$ with respect to α , using Eq. (22) for the fraction of interior counterions. Attempts to fit the data with this approximation yielded lower equilibrium radii and qualitatively different density dependence (dotted black curve in Fig. 6), attributable again to neglect of the macroion electrostatic pressure and to the relatively weak variation of π_{id} with α and ϕ [see Eq. (26)]. However, we find that the uniform ideal-gas approximation may be substantially improved by simply adding the electrostatic pressure associated with the self-energy of a macroion of uniformly distributed net charge $Z_{\text{net}} \equiv Z(1 - f_{\text{in}})$:

$$\beta\pi_{\text{id}}v = Z \left(f_{\text{in}} - (1 - f_{\text{in}}) \frac{\phi}{1 - \phi} \right) + \frac{Z_{\text{net}}^2 \lambda_B}{5a}. \quad (27)$$

For comparison, predictions of Eq. (27) are also plotted in Fig. 6 (dashed black curve). While this heuristic adjustment may prove practical for some purposes, our theory is more accurate and clearly more physically consistent. Despite some potential mismatch between our model of uniformly charged macroions and the core-shell particles studied in ref. [10], and some uncertainty in the variation of local pH inside the microgels and solvency parameter with particle size and concentration, the level of agreement between our theory and experiment is encouraging and should motivate future comparisons.

While Holmqvist *et al.* [10] focused on deionized suspensions by working with microgels that fully ionize at neutral pH and flame-sealing their samples together with an ion exchange resin, other experiments were performed at higher ionic strengths. For example, Borrega *et al.* [4] studied suspensions containing substantial concentrations of sodium chloride (0.01-0.1 M), and Fernández-Nieves *et al.* [6, 7] studied poly-vinylpyridine microgels that fully ionize only at $pH=3$ (ionic strength ~ 1 mM), achieved by adding sodium hydroxide. (Note that addition of NaOH to a sample adjusts pH by promoting acid group ionization, but does not otherwise contribute to the background ion concentration.)

To explore the interrelated effects of varying both particle and salt concentrations, we computed the equilib-

rium swelling ratio over a range of salt concentrations for parameters roughly consistent with the microgels studied in refs. [6] and [7]. We did so by including salt concentration n_s in the Debye screening constant κ and thus in the electrostatic contribution to the internal osmotic pressure π_e [Eq. (24)]. At ionic strengths sufficiently high that background salt ions outnumber counterions dissociated from the particles ($2n_s > Zn_m$), κ and π_e become relatively insensitive to changes in particle concentration. As a consequence, with increasing salt concentration, not only is the degree of swelling reduced, but also the variation of swelling with particle density is weakened, as Fig. 7 illustrates. For reference, the salt-dominated regimes ($2n_s > Zn_m$) are to the left of the dotted curves for respective salt concentrations. By comparison, the uniform ideal-gas approximation [Eq. (26)] predicts $\alpha \simeq 3.6$, independent of ϕ and c_s over these parameter ranges. Our calculations indicate that high background ion concentrations may suppress counterion-induced effects and forestall deswelling until near close packing, where steric interactions between particles become significant. Drawing conclusions about the swelling behavior observed in refs. [6–8] is complicated, however, by the pronounced core-shell structure of the relatively large microgels studied in these experiments – 2-3 times larger than in refs. [4], [5], [9], and [10]. Implementing our theory for a core-shell model of microgels may help to clarify the origins of microgel swelling and deswelling for inhomogeneously structured microgels.

VI. CONCLUSIONS

Based on an exact theorem for the electrostatic contribution to the osmotic pressure inside a permeable macroion, we presented the first rigorous analysis of connections between counterion distribution, osmotic pressure, and particle swelling. As an illustrative example, we applied the new theorem to ionic microgels, explaining observed deswelling of particles with increasing concentration and identifying conditions under which deswelling and narrowing of size polydispersity can be enhanced via redistribution of counterions. This electrostatically-driven phenomenon may be important for tuning rheological properties and facilitating microgel transport through narrow pores in applications ranging from drug delivery to microfluidics to filtration. We validated our results by comparing calculations from nonlinear Poisson-Boltzmann theory with data from molecular dynamics simulations in the spherical cell model. In comparison, theories of macroscopic polyelectrolyte gels, which neglect both spatial variation of the counterion density and the electrostatic pressure of the incompletely neutralized macroion, fail to accurately predict swelling of ionic microgels.

For practical purposes, we also derived a linearized approximation, which provides a convenient analytical expression for the internal electrostatic pressure. By com-

paring predictions with experimental measurements of loosely cross-linked particles in deionized solutions, we demonstrated the ability of our theory to explain and interpret observations of particle swelling in real microgel systems. Our analysis demonstrates, in particular, that soft ionic microgels, when increasingly concentrated, can deswell due to a redistribution of counterions, and confirms that this unusual response can be amplified by increasing particle charge and softness and by minimizing ionic strength. Moreover, we demonstrated that sensitivity of swelling to variations in particle density diminishes with increasing concentration of background ions.

Further comparisons with experiments are possible for

well characterized suspensions of soft, ionic particles. For consistency, however, implementation of our theory should be augmented to incorporate the influence of interparticle interactions between macroions [60], which can be important at concentrations approaching close-packing. Work along these lines is in progress.

ACKNOWLEDGMENTS

This work was supported by the National Science Foundation (Grant No. DMR-1106331). We thank Dr. Jan Dhont for helpful discussions.

-
- [1] D. Vlassopoulos and M. Cloitre, *Curr. Opin. Colloid Interface Sci.* **19**, 561 (2014).
 - [2] A. Fernández-Nieves, A. Fernández-Barbero, B. Vincent, and F. J. de las Nieves, *J. Chem. Phys.* **119**, 10383 (2003).
 - [3] J. J. Liétor-Santos, B. Sierra-Martín, U. Gasser, and A. Fernández-Nieves, *Soft Matter* **7**, 6370 (2011).
 - [4] R. Borrega, M. Cloitre, I. Betremieux, B. Ernst, and L. Leibler, *Euro. Phys. Lett.* **47**, 729 (1999).
 - [5] M. Cloitre, R. Borrega, F. Monti, and L. Leibler, *C. R. Physique* **4**, 221 (2003).
 - [6] A. Fernández-Nieves, A. Fernández-Barbero, B. Vincent, and F. J. de las Nieves, *Macromol.* **33**, 2114 (2000).
 - [7] M. Pelaez-Fernandez, A. Souslov, L. A. Lyon, P. M. Goldbart, and A. Fernández-Nieves, *Phys. Rev. Lett.* **114**, 098303 (2015).
 - [8] G. Romeo, L. Imperiali, J.-W. Kim, A. Fernández-Nieves, and D. A. Weitz, *J. Chem. Phys.* **136**, 124905 (2012).
 - [9] B. H. Tan, K. C. Tam, Y. C. Lam, and C. B. Tan, *J. Rheol.* **48**, 915 (2004).
 - [10] P. Holmqvist, P. S. Mohanty, G. Nägele, P. Schurtenberger, and M. Heinen, *Phys. Rev. Lett.* **109**, 048302 (2012), Erratum, in press (2016).
 - [11] J. J. Liétor-Santos, B. Sierra-Martín, R. Vavrin, Z. Hu, U. Gasser, and A. Fernández-Nieves, *Macromol.* **42**, 6225 (2009).
 - [12] S. M. Hashmi and E. R. Dufresne, *Soft Matter* **5**, 3682 (2009).
 - [13] Y. Hertle, M. Zeiser, C. Hasenöhrl, P. Busch, and T. Hellweg, *Colloid Polym. Sci.* **288**, 1047 (2010).
 - [14] J. J. Liétor-Santos, B. Sierra-Martín, and A. Fernández-Nieves, *Phys. Rev. E* **84**, 060402(R) (2011).
 - [15] B. Sierra-Martín, Y. Laporte, A. B. South, L. A. Lyon, and A. Fernández-Nieves, *Phys. Rev. E* **84**, 011406 (2011).
 - [16] B. Sierra-Martín and A. Fernández-Nieves, *Soft Matter* **8**, 4141 (2012).
 - [17] P. Menut, S. Seiffert, J. Sprakel, and D. A. Weitz, *Soft Matter* **8**, 156 (2012).
 - [18] G. Romeo and M. P. Ciamarra, *Soft Matter* **9**, 5401 (2013).
 - [19] T. G. Mason, J. Bibette, and D. A. Weitz, *Phys. Rev. Lett.* **75**, 2051 (1995).
 - [20] F. Gröhn and M. Antonietti, *Macromol.* **33**, 5938 (2000).
 - [21] Y. Levin, *Phys. Rev. E* **65**, 036143 (2002).
 - [22] A. Fernández-Nieves and M. Márquez, *J. Chem. Phys.* **122**, 084702 (2005).
 - [23] S. P. Singh, D. A. Fedosov, A. Chatterji, R. G. Winkler, and G. Gompper, *J. Phys.: Condens. Matter* **24**, 464103 (2012).
 - [24] R. G. Winkler, D. A. Fedosov, and G. Gompper, *Curr. Opin. Colloid Interface Sci.* **19**, 594 (2014).
 - [25] X. Li, L. E. Sánchez-Díaz, B. Wu, W. A. Hamilton, P. Falus, L. Porcar, Y. Liu, C. Do, A. Faraone, G. S. Smith, T. Egami, and W.-R. Chen, *ACS Macro Lett.* **3**, 1271 (2014).
 - [26] S. A. Egorov, J. Paturej, C. N. Likos, and A. Milchev, *Macromol.* **46**, 3648 (2013).
 - [27] T. Colla, C. N. Likos, and Y. Levin, *J. Chem. Phys.* **141**, 234902 (2014).
 - [28] T. Colla and C. N. Likos, *Mol. Phys.* **113**, 2496 (2015).
 - [29] S. Gupta, M. Camargo, J. Stellbrink, J. Allgaier, A. Radulescu, P. Lindner, E. Zaccarelli, C. N. Likos, and D. Richter, *Nanoscale* **7**, 13924 (2015).
 - [30] S. Gupta, J. Stellbrink, E. Zaccarelli, C. N. Likos, M. Camargo, P. Holmqvist, J. Allgaier, L. Willner, and D. Richter, *Phys. Rev. Lett.* **115**, 128302 (2015).
 - [31] L. A. Lyon and M. J. Serpe, eds., *Hydrogel Micro and Nanoparticles* (Wiley-VCH Verlag GmbH & Co. KGaA, Weinheim, 2012).
 - [32] A. Fernández-Nieves, H. Wyss, J. Mattsson, and D. A. Weitz, eds., *Microgel Suspensions: Fundamentals and Applications* (Wiley-VCH Verlag GmbH & Co. KGaA, Weinheim, 2011).
 - [33] L. A. Lyon and A. Fernández-Nieves, *Annu. Rev. Phys. Chem.* **63**, 25 (2012).
 - [34] P. J. Yunker, K. Chen, D. Gratale, M. A. Lohr, T. Still, and A. G. Yodh, *Rep. Prog. Phys.* **77**, 056601 (2014).
 - [35] W. O. Baker, *Ind. Eng. Chem.* **41**, 511 (1949).
 - [36] R. H. Pelton and P. Chibante, *Colloids Surf.* **20**, 247 (1986).
 - [37] R. H. Pelton, *Adv. Colloid Interface Sci.* **85**, 1 (2000).
 - [38] B. R. Saunders, N. Laajam, E. Daly, S. Teow, X. Hu, and R. Stepto, *Adv. Colloid Interface Sci.* **147**, 251 (2009).
 - [39] R. Pelton and T. Hoare, in *Microgel Suspensions: Fundamentals and Applications*, edited by A. Fernández-Nieves, H. Wyss, J. Mattsson, and D. A. Weitz (Wiley-VCH Verlag GmbH & Co. KGaA, Weinheim, 2011) pp. 3–32.

- [40] R. K. Shah, J.-W. Kim, J. J. Agresti, D. A. Weitz, and L.-Y. Chu, *Soft Matter* **4**, 2303 (2008).
- [41] T. Still, K. Chen, A. M. Alsayed, K. B. Aptowicz, and A. G. Yodh, *J. Colloid Interface Sci.* **405**, 96 (2013).
- [42] M. Hamidi, A. Azadi, and P. Rafiei, *Advanced Drug Delivery Rev.* **60**, 1638 (2008).
- [43] J. K. Oh, R. Drumright, D. J. Siegwart, and K. Matyjaszewski, *Prog. Polym. Sci.* **33**, 448 (2008).
- [44] J. K. Oh, D. I. Lee, and J. M. Park, *Prog. Polym. Sci.* **34**, 1261 (2009).
- [45] S. Schmidt, P. A. L. Fernandes, B. G. D. Geest, M. Delcea, A. G. Skirtach, H. Möhwald, and A. Fery, *Adv. Funct. Mater.* **21**, 1411 (2011).
- [46] D. Sivakumaran, D. Maitland, T. Oszustowicz, and T. Hoare, *J. Colloid Interface Sci.* **392**, 422 (2013).
- [47] P. S. Mohanty and W. Richtering, *J. Phys. Chem. B* **112**, 14692 (2008).
- [48] T. Eckert and W. Richter, *J. Chem. Phys.* **129**, 124902 (2008).
- [49] A. N. St. John, V. Breedveld, and L. A. Lyon, *J. Phys. Chem. B* **111**, 7796 (2007).
- [50] M. Muluneh and D. A. Weitz, *Phys. Rev. E* **85**, 021405 (2012).
- [51] J. Riest, P. Mohanty, P. Schurtenberger, and C. N. Likos, *Z. Phys. Chem.* **226**, 711 (2012).
- [52] P. S. Mohanty, A. Yethiraj, and P. Schurtenberger, *Soft Matter* **8**, 10819 (2012).
- [53] D. Paloli, P. S. Mohanty, J. J. Crassous, E. Zaccarelli, and P. Schurtenberger, *Soft Matter* **9**, 3000 (2013).
- [54] U. Gasser, J.-J. Liétor-Santos, A. Scotti, O. Bunk, A. Menzel, and A. Fernández-Nieves, *Phys. Rev. E* **88**, 052308 (2013).
- [55] P. S. Mohanty, D. Paloli, J. J. Crassous, E. Zaccarelli, and P. Schurtenberger, *J. Chem. Phys.* **140**, 094901 (2014).
- [56] A. R. Denton, *Phys. Rev. E* **67**, 011804 (2003), **68**, 049904(E) (2003).
- [57] D. Gottwald, C. N. Likos, G. Kahl, and H. Löwen, *J. Chem. Phys.* **122**, 074903 (2005).
- [58] C. N. Likos, in *Microgel Suspensions: Fundamentals and Applications*, edited by A. Fernández-Nieves, H. Wyss, J. Mattsson, and D. A. Weitz (Wiley-VCH Verlag GmbH & Co. KGaA, Weinheim, 2011) pp. 165–193.
- [59] V. A. Baulin and E. Trizac, *Soft Matter* **8**, 6755 (2012).
- [60] M. M. Hedrick, J. K. Chung, and A. R. Denton, *J. Chem. Phys.* **142**, 034904 (2015).
- [61] G. C. Claudio, K. Kremer, and C. Holm, *J. Chem. Phys.* **131**, 094903 (2009).
- [62] M. Quesada-Pérez and A. Martín-Molina, *Soft Matter* **9**, 7086 (2013).
- [63] S. Schneider and P. Linse, *Eur. Phys. J. E* **8**, 457 (2002).
- [64] H. Kobayashi and R. G. Winkler, *Polymers* **6**, 1602 (2014).
- [65] H. Kobayashi and R. G. Winkler, *Sci. Rep.* **6**, 19836 (2016).
- [66] H. H. Hooper, J. P. Baker, H. W. Blanch, and J. M. Prausnitz, *Macromol.* **23**, 1096 (1990).
- [67] A. E. English, S. Mafé, J. A. Manzanares, X. Yu, A. Y. Grosberg, and T. Tanaka, *J. Chem. Phys.* **104**, 8713 (1996).
- [68] G. Nisato, J. P. Munch, and S. J. Candau, *Langmuir* **15**, 4236 (1999).
- [69] A. Fernández-Nieves, A. Fernández-Barbero, and F. J. de las Nieves, *J. Chem. Phys.* **115**, 7644 (2001).
- [70] T. López-León, J. L. Ortega-Vinuesa, D. Bastos-González, and A. Elaissari, *J. Phys. Chem. B* **110**, 4629 (2006).
- [71] D. Capriles-González, B. Sierra-Martín, A. Fernández-Nieves, and A. Fernández-Barbero, *J. Phys. Chem. B* **112**, 12195 (2008).
- [72] P. J. Flory, *Principles of Polymer Chemistry* (Cornell University Press, Ithaca, 1953).
- [73] A. Katchalsky, S. Lifson, and H. Eisenberg, *J. Polym. Sci. A* **7**, 571 (1951).
- [74] A. Katchalsky and I. Michaeli, *J. Polym. Sci. A* **15**, 69 (1955).
- [75] P.-G. de Gennes, *Scaling Concepts in Polymer Physics* (Cornell, Ithaca, 1979).
- [76] J.-L. Barrat, J.-F. Joanny, and P. Pincus, *J. Phys. II France* **2**, 1531 (1992).
- [77] M. Rubinstein, R. H. Colby, A. V. Dobrynin, and J.-F. Joanny, *Macromol.* **29**, 398 (1996).
- [78] E. Y. Kramarenko, A. R. Khokhlov, and K. Yoshikawa, *Macromol.* **30**, 3383 (1997).
- [79] M. Malmsten, in *Microgel Suspensions: Fundamentals and Applications*, edited by A. Fernández-Nieves, H. Wyss, J. Mattsson, and D. A. Weitz (Wiley-VCH Verlag GmbH & Co. KGaA, Weinheim, 2011) pp. 375–405.
- [80] K. N. Nordstrom, E. Verneuil, P. E. Arratia, A. Basu, Z. Zhang, A. G. Yodh, J. P. Gollub, and D. J. Durian, *Phys. Rev. Lett.* **105**, 175701 (2010).
- [81] A. Bouchoux, P. Qu, P. Bacchin, and G. Gésan-Guiziou, *Langmuir* **30**, 22 (2013).
- [82] R. Roa, E. K. Zholkovskiy, and G. Nägele, *Soft Matter* **11**, 4106 (2015).
- [83] G. S. Manning, *J. Chem. Phys.* **51**, 924 (1969).
- [84] R. A. Marcus, *J. Chem. Phys.* **23**, 1057 (1955).
- [85] A. R. Denton, *J. Phys.: Condens. Matter* **22**, 364108 (2010).
- [86] Y. Hallez, J. Diatta, and M. Meireles, *Langmuir* **30**, 6721 (2014).
- [87] M. Urich and A. R. Denton, unpublished.
- [88] H. Wennerström, B. Jönsson, and P. Linse, *J. Chem. Phys.* **76**, 4665 (1982).
- [89] M. Deserno and C. Holm, in *Electrostatic Effects in Soft Matter and Biophysics*, NATO Advanced Studies Institute, Series II: Mathematics Physics and Chemistry, Vol. 46, edited by C. Holm, P. Kékicheff, and R. Podgornik (Kluwer, Dordrecht, 2001) pp. 27–50.
- [90] S. Plimpton, *J. Comp. Phys.* **117**, 1 (1995).
- [91] <http://lammmps.sandia.gov>.
- [92] M. Stieger, W. Richtering, J. S. Pedersen, and P. Lindner, *J. Chem. Phys.* **120**, 6197 (2004).
- [93] A. M. Rumyantsev, A. A. Rudov, and I. I. Potemkin, *J. Chem. Phys.* **142**, 171105 (2015).